Title: Vapor deposition of a nonmesogen prepares highly structured organic glasses

Authors:

1. Camille Bishop, cbishop4@wisc.edu
   Department of Chemistry, University of Wisconsin – Madison
2. Jacob L. Thelen, jacob.thelen@nist.gov
   The National Institute of Standards and Technology (NIST)
3. Eliot Gann, eliot.gann@nist.gov
   The National Institute of Standards and Technology (NIST)
4. Michael F. Toney, mftoney@slac.stanford.edu
   Stanford Synchrotron Radiation Lightsource, SLAC National Accelerator Laboratory
5. Lian Yu, lian.yu@wisc.edu
   School of Pharmacy, University of Wisconsin – Madison
6. Dean M. DeLongchamp, dean.delongchamp@nist.gov
   The National Institute of Standards and Technology (NIST)
7. M. D. Ediger, ediger@chem.wisc.edu
   Department of Chemistry, University of Wisconsin – Madison

Significance statement

Organic glasses are useful, versatile materials for current and future organic electronic technologies. They are non-equilibrium materials, so a single-component system can be processed in different ways to create a wide range of solids with diverse structural and optical properties. In this work, we use physical vapor deposition to prepare glasses with structure similar to that of an aligned smectic liquid crystal from a molecule that does not have any liquid crystal phases. This shows the potential to create highly structured glasses from a wide range of molecules.

Abstract

We show that glasses with aligned smectic liquid crystal-like order can be produced by physical vapor deposition of a molecule without any equilibrium liquid crystal phases. Smectic-like order in vapor-deposited films was characterized by wide-angle X-ray scattering. A surface equilibration mechanism predicts the highly smectic-like vapor-deposited structure to be a result of significant vertical anchoring at the surface of the equilibrium liquid, and NEXAFS spectroscopy orientation analysis confirms this prediction. Understanding of the mechanism enables informed engineering of different levels of smectic order in vapor-deposited glasses to suit various applications. The preparation of a glass with orientational and translational order from a non-liquid crystal opens up an exciting new paradigm for accessing extreme anisotropy in glassy solids.

Introduction

While glasses are sometimes characterized as "randomly packed" and lacking "structure", in reality glasses can show a wide range of interesting and useful packing motifs. Because glasses are out-of-equilibrium, there are in principle an essentially infinite number of structurally distinct, mechanically stable glassy solids even for a single-component system. While many of these different glasses will have similar properties, it has been shown that significant variations in properties such as density (1), stress response (2), and thermal stability (3) can be achieved in glasses of single-component systems. Ultimately, these property differences result from different glass structures.

One of the most interesting and useful aspects of structure in glasses is anisotropy. There are many ways to induce anisotropy in glasses, such as thermomechanical processing of polymer (4) and metallic (5) glasses, or physical vapor deposition of organic (6, 7) and inorganic (8) systems. For organic glasses, orientational anisotropy allows modulation of light absorption and emission, and anisotropic packing with nearest neighbors modulates charge mobility. Anisotropic glasses have been successfully used in applications such as organic light-emitting diodes (OLEDs) (9), and are increasingly being explored for other emerging organic electronics, including field-effect transistors (10, 11) and photovoltaics (12). In contrast to the difficulty of growing large single crystals with controlled orientation, macroscopically aligned glasses without grain boundaries can easily be produced (13). Glasses can also readily incorporate guest

species without disrupting macroscopic homogeneity (14, 15). Since anisotropic glasses combine the processing advantages of glasses with anisotropy that yields favorable electronic and optical properties, they are promising for future technology such as flexible and printed devices (16).

There has been considerable interest in using liquid crystals to produce highly anisotropic glasses and several preparation routes have been explored (17). When a liquid crystal is cooled, a frozen version of its structure is formed, unless nucleation into a 3D crystal occurs first. The solid formed by the liquid crystal-cooling route will include strong orientational (18), and possibly translational (19), correlation between neighboring molecules. If the liquid crystal is aligned along a common direction before cooling by using alignment layers or an electromagnetic field (20), the solid that is formed will have strongly anisotropic local and macroscopic structure. Vapor deposition of molecules with liquid crystalline phases has recently been identified as another method for producing highly anisotropic, macroscopically aligned glasses with both orientational (13, 21) and translational (22, 23) order. Glasses prepared with liquid crystalline order have enhanced charge mobility (24, 25) compared to their isotropic counterparts.

In this work, we identify a new route for producing highly anisotropic glasses with orientational and translational order similar to that of a smectic liquid crystal. In contrast to the examples discussed above, we show that smectic-like glasses can be achieved using a molecule (posaconazole) which does not have any equilibrium liquid crystal phases. We characterize the molecular packing of the glasses by grazing-incidence wide-angle X-ray scattering (GIWAXS) (26, 27). Using near-edge X-ray absorption fine structure (NEXAFS) spectroscopy, we determine the molecular orientation at the free surface of an isotropic glass prepared by cooling the equilibrium liquid. We find that the high level of order at the free surface of posaconazole allows the deposition of glasses with significant smectic-like ordering. With this result, we recognize that even molecules that do not form liquid crystals can have extremely anisotropic locally ordered solid packing arrangements reminiscent of liquid crystal phases. There is every reason to expect that there are many organic molecules with the potential to form glasses with similar liquid crystalline anisotropy, if the right preparation method can be identified.

Results

While our main results concern vapor-deposited glasses of posaconazole, the isotropic liquid-cooled glass of posaconazole is an important point of reference. The molecular structure of posaconazole is shown in Figure 1A. Above its glass transition temperature, T_g, posaconazole is an isotropic liquid (21). When a glass is formed by cooling the equilibrium liquid to room temperature from 334 K (T_g + 4 K), it inherits the structure of the isotropic equilibrium liquid, as shown in the GIWAXS pattern in Figure 1B. The sole feature in the X-ray diffraction of the liquid-cooled glass of posaconazole is a broad amorphous peak around $q \approx 1.3$ Å^{-1} that is equally distributed azimuthally. We associate this with the distance of closest lateral approach between neighboring rods (≈ 0.48 nm). An illustration of the structure of the isotropic liquid-cooled glass is presented in Figure 1C.

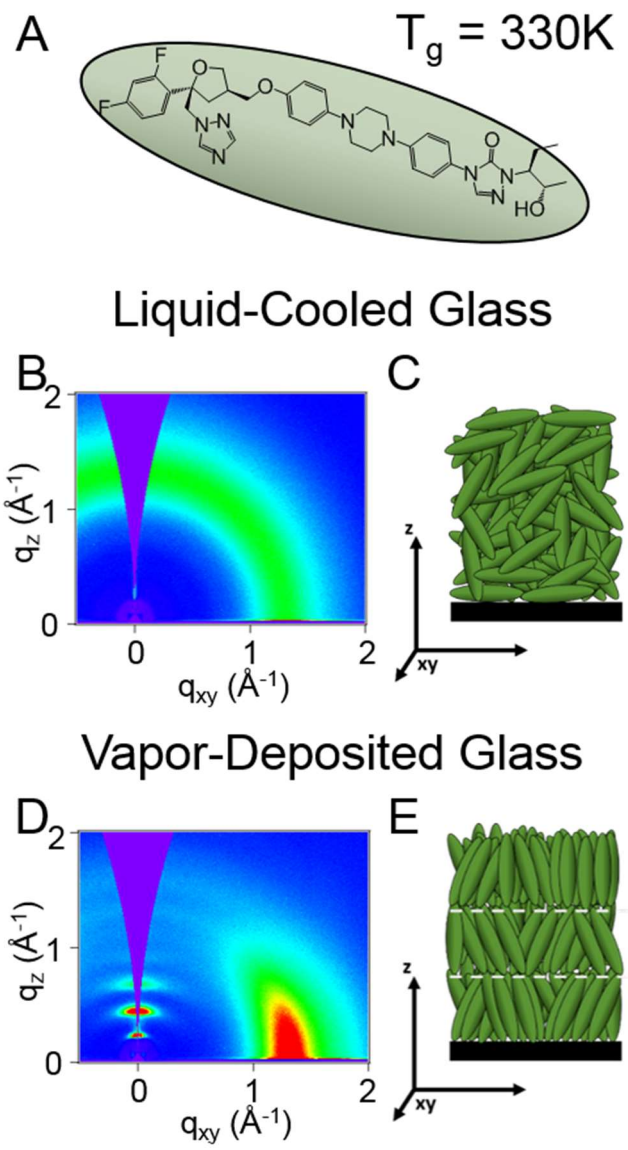

Figure 1. X-ray scattering of liquid-cooled and vapor-deposited glasses of posaconazole shows that high levels of smectic-like order are accessible only through vapor deposition. (A) Molecular structure of posaconazole, which has a glass transition at 330 K. (B) Grazing incidence wide-angle X-ray scattering (GIWAXS) of liquid-cooled posaconazole is consistent with an isotropic glass, as illustrated in (C). (D) GIWAXS of posaconazole vapor-deposited at 324 K at 0.02 nm s^{-1} reveals smectic-like translational order and nematic-like orientational order, as illustrated in (E).

When vapor deposited, posaconazole produces a glass with significant smectic-like order that is not present in the liquid-cooled glass. By vapor-depositing at a rate of 0.02 nm s^{-1} on a silicon substrate held at 324 K, a glass with the X-ray scattering pattern shown in Figure 1D is produced. In contrast to the liquid-cooled glass, the vapor-deposited glass has a high level of translational smectic-like order, which produces the intense peaks at q_z values of ~(0.2, 0.4, and 0.6) $Å^{-1}$. These three peaks resemble those of the equilibrium smectic liquid crystal itraconazole (28, 29), suggesting that the order in the vapor-deposited glass of posaconazole is smectic-like. Corrected for instrumental broadening, the Scherrer correlation length of the peak at $q_z \approx 0.4$ $Å^{-1}$ is 18.4 nm, which is equal to approximately six molecular lengths. The vapor-deposited glass also has a high degree of orientational order consistent with smectic-like packing, as evidenced by the localized azimuthal distribution of the broad peak at $q \approx 1.3$ $Å^{-1}$. Rather than being isotropic, the scattering from the lateral packing of neighboring rods is focused in-plane, consistent with the structure illustrated in Figure 1E. The high degree of orientational order as revealed by X-ray scattering is consistent with previous birefringence and IR absorption data on vapor-deposited posaconazole (21). The correlation length from this broad peak, corrected for instrumental broadening, is 2.9 nm, which is equal to approximately six molecules arranged laterally in-plane; this small correlation length is consistent with the view that the vapor-deposited film is not a 3D crystal. Despite posaconazole having no known nematic or smectic phases, the vapor-deposited glass shows features similar to those of an aligned smectic liquid crystal (22).

To understand the origin of the structure of the vapor-deposited glass, we investigate the equilibrium liquid. A surface equilibration mechanism has been proposed to explain the unique properties of vapor-deposited glasses (1, 6, 8). The surface of an organic glass can be much more mobile than the bulk, with diffusion coefficients that can be up to eight orders of magnitude larger (30). During deposition, each deposited molecule resides at the free surface for (typically) a few seconds, during which the molecules utilize enhanced surface mobility to equilibrate towards the structure of the (metastable) equilibrium liquid. As the deposition progresses, the partially (or fully) equilibrated molecules become buried in the bulk glass with relaxation times that exceed accessible experimental time scales. While we expect that vapor deposition of posaconazole follows this surface equilibration mechanism, the vapor-deposited structure (Figure 1D and 1E) has a high degree of concurrent orientational and translational order atypical of other

non-liquid crystalline systems studied to date (27, 31, 32). Therefore, we infer that posaconazole must have a different surface structure during deposition than other systems studied thus far.

Because the surface equilibration mechanism predicts that the structure of vapor-deposited posaconazole depends upon the surface structure of the equilibrium liquid, we use NEXAFS spectroscopy to study the molecular orientation at the surface. We performed incident angle-dependent NEXAFS (33) on the liquid-cooled glass at the carbon K-edge. We expect that the liquid-cooled glass has a structure that accurately approximates that of the equilibrium liquid just above T_g. Within the energy range shown in Figure 2A, we note several main features. Peaks around 285.2, 286.7, and 287.5 eV correspond to the 1s → π* transitions for the aromatic phenyl, C=N bonds in triazole (34), and C=CF bonds in fluorobenzene rings (35, 36), respectively. Our C=CF peak assignment is supported by the absence of this peak system in NEXAFS spectroscopy of itraconazole (SI text, NEXAFS orientation and peak analysis), which lacks fluorobenzene rings. The peak at 289.6 eV is assigned to the 1s→π* carbonyl transition (37), while a broad peak around ~294 eV corresponds to the 1s→σ* carbon-carbon resonance. The sharp transitions at energies below ~290 eV provide sufficient signal-to-noise to determine incident angle-dependent absorption, so we use these resonances to report the orientation of the central core of posaconazole. Data was collected in partial electron yield mode with a grid bias of -219 V, and we therefore expect the NEXAFS measurements to probe roughly the top 6 nm of the free surface, which is approximately two molecular layers.

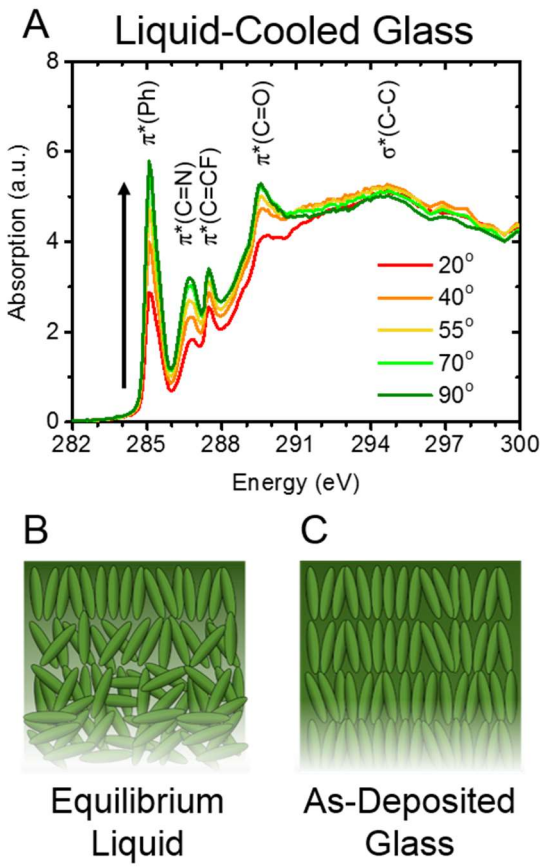

Figure 2. Near-edge X-ray absorption fine structure (NEXAFS) spectroscopy shows that the molecules at the free surface of the liquid-cooled glass, and therefore the equilibrium liquid of posaconazole, are vertically oriented. (A) NEXAFS at the carbon K-edge for a liquid-cooled posaconazole glass, deposited as an equilibrium isotropic liquid at 334 K and cooled to room temperature at 1 K min^{-1}. (B) Illustration of the proposed surface structure of the posaconazole liquid. The top layer of posaconazole molecules is oriented with an average long axis tilt of ~33° from the surface normal (SI text, NEXAFS orientation and peak analysis). This anisotropy is present only at the surface, and gives way to an isotropic bulk revealed by ellipsometry (SI text, Bulk orientation of liquid-cooled glass). (C) When vapor-deposited, the molecular orientation throughout the bulk of the glass resembles that of the surface of the equilibrium liquid.

The molecules at the free surface of posaconazole show strong vertical orientation in contrast to the random orientation in the bulk of the liquid-cooled glass. Figure 2A shows the incident angle-dependent partial electron yield NEXAFS spectra of the liquid-cooled glass (deposited into the equilibrium liquid at 334 K and subsequently cooled to room temperature at

1 K min^{-1}). Changing the incident angle of p-polarized light alters the angle of the electric field vector relative to the 1s→π* transition dipole vectors. For the 1s→π* resonances, the maximum intensity occurs when p-polarized radiation is at normal incidence to the substrate, and the minimum occurs at lower incidence angles. This is consistent with a 1s→π* transition dipole vector orientation preferentially parallel to the substrate; our fit to the data provides an angle of 57° between the 1s→π* transition dipole and surface normal.

We can connect the 1s→π* transition dipole orientation to the posaconazole long axis orientation by modeling posaconazole as a rod, such that the vectors normal to the conjugated planes of its core equally adopt all possible orientations orthogonal to the long molecular axis. This assumption is supported by our GIWAXS data in Figure 1D, which has a broad peak at q_{xy} ≈ 1.3 $Å^{-1}$ that occurs at too large of a d-spacing to be associated with a pi-pi stacking interaction. This allows us to rule out posaconazole orientations where the molecular long axis is lying down with its conjugated plane "edge on" upon the substrate. Strong vertical orientation of the long molecular axis is further supported by the behavior of some of the other resonances in the spectra shown in Figure 2, particularly the carbon-carbon 1s→σ*, which exhibits an out-of-plane orientation preference consistent with a vertical long axis. Modeling posaconazole as a rod allows an analysis identical to that of a planar orbital with high substrate symmetry (33). Using this approach, we solve for an average angle of ~33° between the posaconazole long axis and surface normal (SI text, NEXAFS orientation and peak analysis). The surface orientation of posaconazole is different from that revealed by simulations of other organic molecules, which tend to exhibit mild perpendicular orientation at the free surface (38, 39). We infer that this highly vertical orientation of the long axis at the free surface is therefore responsible for the high degree of orientational order seen in the vapor-deposited glass. It was previously hypothesized that posaconazole may have a highly oriented surface structure similar to that observed in nematic liquid crystals (21, 40); Figure 2 confirms that hypothesis. The isotropic *bulk* structure of the liquid-cooled glass of posaconazole is indicated in Figure 1B and was further confirmed by ellipsometry (SI text, Bulk orientation of liquid-cooled glass) (21).

Both the substrate temperature and deposition rate can be changed to manipulate the precise structure of vapor-deposited glasses of posaconazole. GIWAXS of three vapor-deposited posaconazole glasses are shown in Figure 3. Each of the glasses shown has a different layer d-

spacing and a different degree of orientational order, as shown in Figure 3D. With just a single order of magnitude increase in deposition rate at 325 K, the layering peak moves from q = 0.219 to 0.232 Å^{-1}, which corresponds to a 6% decrease in layer d-spacing from (2.87 to 2.71) nm. The orientational order varies greatly from glass to glass, even in the narrow temperature and deposition rate window presented here. Given a wide range of deposition conditions, the structure of posaconazole can be continuously varied to create a range of solids with differing structural, and therefore mechanical (2) and optical (41) properties.

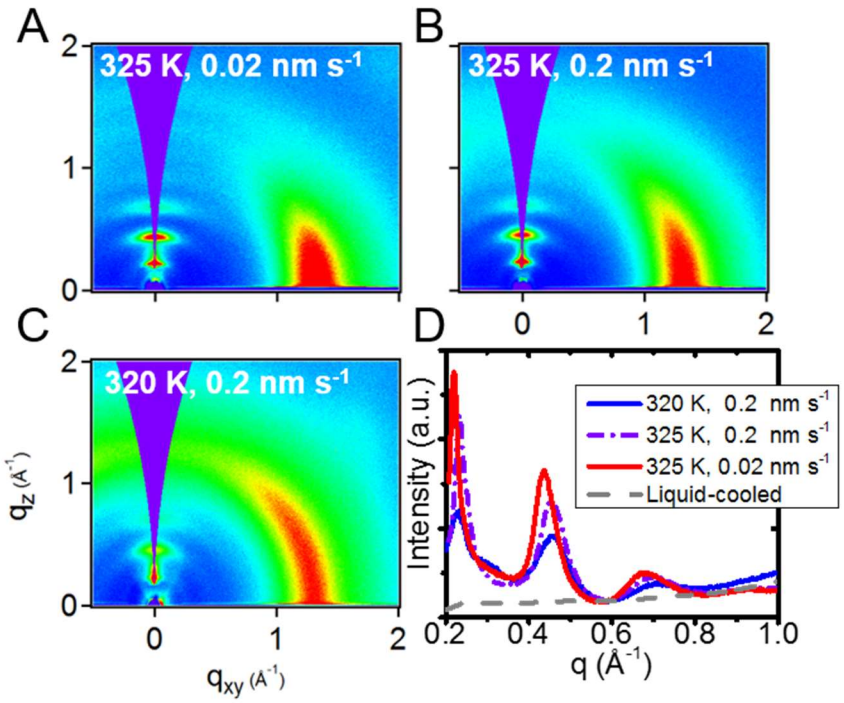

Figure 3. Vapor deposition can produce a wide range of structures that depend upon both substrate temperature and deposition rate. (A) through (C) are GIWAXS patterns from vapor-deposited glasses of posaconazole, with various degrees of order depending on deposition conditions. Two-dimensional patterns show different amounts of translational and orientational order from different combinations of substrate temperature and deposition rate. (D) One-dimensional integrations near q_z for two-dimensional patterns in (A) through (C), which show the degree and spacing of smectic-like ordering. A liquid-cooled glass, prepared by cooling the liquid from 334 K, is shown for reference.

The effects of changing the substrate temperature and deposition rate can be explained by the surface equilibration mechanism (6, 31), which posits that the structure and mobility at the

free surface of the glass during deposition is responsible for the structure of the bulk vapor-deposited glass. Comparing the glasses prepared at 0.2 nm s^{-1} at 320 K and 325 K (Figures 3B and 3C), the glass deposited at a higher substrate temperature has greater orientational order, shown by the increased azimuthal localization of the broad peak at $q \approx 1.3$ $Å^{-1}$ into the near-q_{xy} direction (SI text, bulk orientational order of vapor-deposited glass). At higher substrate temperatures, molecules at the surface can more thoroughly equilibrate towards the equilibrium surface structure before becoming locked into the glassy bulk (30). (A change in the substrate temperature may also change the tilt angle at the equilibrium free surface; in this work, we assume the equilibrium surface orientation to be approximately constant over the range of substrate temperatures shown.) Comparing Figure 3A and 3B, the glass deposited at a lower rate (Figure 3A) shows a further increase in order as each molecule spends more time at the highly mobile free surface (42, 43). Therefore, given a highly orientationally ordered equilibrium free surface, lower deposition rates and higher substrate temperatures result in glasses with more ordered molecules. The molecular orientation at the free surface derived from NEXAFS provides an approximate upper bound on vertical molecular orientation in the vapor-deposited glass. We may estimate the molecular orientation in the bulk glass using the out-of-plane peak spacing by approximating the molecules as 3.2 nm (44) rigid rods. Assuming that the layer spacing is caused by molecular tilt, the molecules in the glass prepared at the highest substrate temperature and lowest rate (Figure 3A) have long axes tilted approximately 26° from the surface normal, roughly consistent with the orientation determined by NEXAFS. The sharpening of the peaks at q values of ~(0.2, 0.4, and 0.6) $Å^{-1}$ for the glass deposited at higher substrate temperature and lower rates indicates a growing coherence length of out-of-plane translational ordering (45).

We attribute the translational order in the vapor-deposited glasses to two possible origins. Translational order at the free surface of the liquid may persist beyond the top layer of molecules as indicated by Figure 2B. The NEXAFS measurements cannot provide direct evidence for this translational order, but such order has been observed at the equilibrium free surface of other non-liquid crystalline systems (31, 46). Deposition would naturally trap this layered structure into the glass. Alternately, it is possible that a layered glass might be formed solely on the basis of a strong tendency for vertical alignment in the topmost liquid layer. In this case, equilibration during deposition would try to create a top layer of vertically oriented molecules. Once complete coverage was achieved, subsequently deposited molecules might begin to create new layers,

while leaving those below undisturbed. Molecular dynamics computer simulations of the vapor deposition process might succeed in distinguishing between these two explanations (38, 47).

Despite having highly organized molecular packing, vapor-deposited solids of posaconazole are not crystalline, as shown by their evolution during annealing. We prepared a posaconazole glass at a rate of 0.02 nm s^{-1} on a substrate held at 325 K, and then annealed it isothermally at 335 K (T_g + 5 K). The complete experiment is detailed in "Materials and Methods". As shown in Figure 4, the highly ordered vapor-deposited glass transforms irreversibly into the isotropic liquid when held slightly above T_g (and far below the crystal melting point of 443 K). Figure 4 shows the loss of translational and orientational order requires less than 400 seconds. In contrast, if 3D crystals were responsible for the order in the vapor-deposited materials, we would observe sharpening of the peaks during annealing as the crystals grew in size; no sharp peaks are observed in the two-dimensional patterns in Figures 4A through 4C. When the sample shown in Figure 4 was cooled at 1 K min^{-1} after annealing, the glass remained isotropic, indicating an irreversible transformation. The transformation from ordered glass to isotropic liquid shown in Figure 4 takes roughly 300 times as long as the transformation from ordinary glass to isotropic liquid (44); this result is similar to what has been observed for other PVD glasses (21, 48).

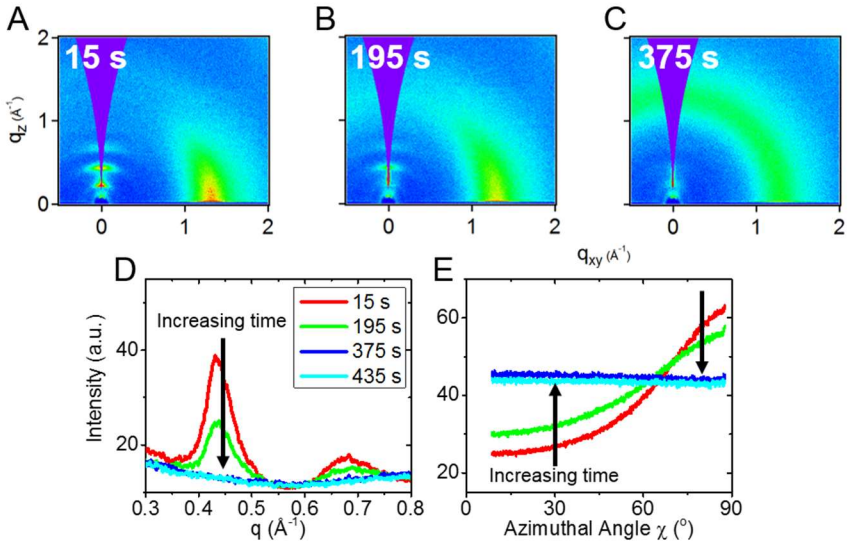

Figure 4. Vapor-deposited posaconazole glasses irreversibly transform into the isotropic supercooled liquid when held well below the crystal melting point. (A) through (C) show GIWAXS from 30-second exposures of a posaconazole glass vapor-deposited at 325 K and 0.02 nm s^{-1} during annealing at 335 K. (D) Integrations near q_z show the decay of smectic-like order during annealing. (E) Radial integrations of the broad peak around $q \approx 1.3$ $Å^{-1}$ show the decay of orientational nematic order during annealing.

Discussion

The striking order shown by vapor-deposited glasses of posaconazole (Figures 1 and 3), characteristic of an aligned smectic liquid crystal, is remarkable in light of the absence of equilibrium liquid crystal phases for this molecule. These are the most highly structured glasses ever produced from non-mesogens. Our work highlights the ability of vapor deposition to produce highly anisotropic non-equilibrium packing arrangements that cannot at present be attained with other methods. We anticipate that this work will extend the range of systems from which highly anisotropic glasses can be prepared.

It will be important to refine strategies for the identification of additional non-mesogens that, similar to posaconazole, can produce highly ordered glasses. The amphiphilic nature of posaconazole may be responsible for its vertical orientation at the surface of the free liquid. In recent simulations of vapor-deposited glasses of amphiphilic fluorinated molecules, the fluorinated tails segregate to the surface (49); it is plausible that posaconazole behaves similarly during deposition and this provides a guide in selecting additional systems for study. Our investigation of posaconazole was motivated by its structural similarity with itraconazole, a system known to form smectic liquid crystals. This suggests that it would be fruitful to investigate additional sets of structurally similar molecules that contain both mesogens and non-

mesogens. More generally, molecular dynamics computer simulations have proven useful for understanding the surface structure of liquids (31, 39, 50) and these could be employed to screen additional candidates. It would be particularly interesting to identify candidates with disk-like cores that might result in glasses with columnar order.

We anticipate that these glasses with high, tunable levels of orientational and translational order may be useful for new applications in organic electronics. The non-equilibrium nature of these materials means that for a single molecular system, precise properties of the glass can be "dialed in" by changing the rate and substrate temperature during deposition. The surface equilibration mechanism can be used to predict the correct deposition parameters for the desired application. Liquid crystalline order has been shown to produce enhanced charge mobility (24, 25) and unique optoelectronic properties (16, 24, 51, 52). We anticipate that the new solids prepared by the route described here combine the advantages of anisotropic glasses produced from liquid crystals with the compositional flexibility and macroscopic homogeneity of liquid-cooled glasses, making them important materials for the next generation of devices.

Materials and Methods

Posaconazole VETRANAL analytical standard was used as-received from Sigma Aldrich.[*] Samples were prepared in a custom-built vacuum chamber at a base pressure of 10^{-6} Torr. The source to substrate distance was 11 cm (21). Samples prepared for GIWAXS ranged in thickness from 300-450 nm, with the exception of those shown in Figure 1, which are 1μm thick. Previous work has shown that, above 100 nm, bulk properties are independent of film thickness (6, 21). Samples prepared for NEXAFS were slightly thinner (~70 nm), to avoid sample charging

[*] Certain commercial equipment, instruments, or materials (or suppliers, or software, ...) are identified in this paper to foster understanding. Such identification does not imply recommendation or endorsement by the National Institute of Standards and Technology, nor does it imply that the materials or equipment identified are necessarily the best available for the purpose.

effects which can introduce artifacts (53). All samples for both techniques were prepared on identical 1-inch undoped silicon <1 0 0> wafers with 2 nm native oxide (Virginia Semiconductor).

GIWAXS was performed at beamline 11-3 at the Stanford synchrotron radiation lightsource (SSRL). Scans were acquired at an incidence angle of $\theta_{in} = 0.14°$, which is above the critical angle for posaconazole. The X-ray energy is 12.7 keV, with a sample-to-detector distance of 315 mm. When calculating instrumental broadening, a 25 mm spot size was assumed to account for a grazing-incidence footprint on a 25 mm wafer. Scans were performed in a Helium atmosphere. As-deposited and liquid-cooled scattering patterns were collected using exposure times of 120 s. Data was reduced using the WAXStools plugin (54) in the Nika 2D SAS package for Igor Pro (55, 56). Smectic-like order integrations (Figures 3D, 4E) were taken near q_z, rather than directly along q_z, since scattering from directly along q_z is unavailable from grazing incidence geometry (57). Scans were integrated between azimuthal angle $\chi = 4°$ to 8°, and $\chi = -4°$ to -8°, where $\chi = 0°$ is along q_z. For each scan, the two integrations were summed, and normalized by the average film thickness determined by spectroscopic ellipsometry (J.A. Woollam M-2000U).

NEXAFS data were collected using the Soft X-ray Spectroscopy beamline at the Australian synchrotron (AS). Scans were performed using linearly polarized X-rays and five different sample tilt angles, such that the electric field vector was aligned at $\theta_{in} = 90°$, 70°, 55°, 40°, and 20° relative to the sample surface normal. X-ray absorption was monitored using the channeltron detector operating in partial electron yield mode (PEY) with a bias of -219 V. Scans were recorded over an energy range of 230-430 eV. The data were corrected and analyzed using the Quick AS NEXAFS Tool (QANT) (58). Each scan was corrected for energy offset by normalizing to the highly oriented pyrolyzed graphite (HOPG) internal standard. The absorption values were corrected using both the gold mesh instantaneous flux monitor and a photodiode secondary reference. After corrections, each scan was normalized using the empirical step method described by Gann et al. (58); the pre-edge intensity values were scaled to 0 by subtracting the average absorption between 275-280 eV, and the post-edge intensity values were scaled to 1. The normalized scans were analyzed using the multipeak fit function in QANT. The data between 275-390eV were well-fit by the sum of an “edge” baseline and nine Gaussian

peaks. The peak positions and widths, determined by fitting the θ_{in} = 55° dataset, were held constant, while the peak heights were fitted for each sample. The fit results are provided in SI text, NEXAFS orientation and peak analysis.

To prepare liquid-cooled glasses, two methods were used. For the liquid-cooled glass used for GIWAXS, shown in Figure 1B, a 1100 nm-thick glass of posaconazole deposited at 329 K at 0.2 nm s^{-1} was held at 334 K in a He atmosphere for 10 minutes. It was then cooled at a rate of 1 K min^{-1} to 328 K, then brought to room temperature at ambient conditions. For NEXAFS, the liquid-cooled glass was prepared by vapor depositing directly at 334 K in vacuum. After deposition, the liquid was immediately cooled to 320 K at a rate of 1 K min^{-1}, after which it was brought to room temperature at 5 K min^{-1}. Bulk isotropy of the glass was confirmed using spectroscopic ellipsometry (SI text, Bulk orientation of liquid-cooled glass).

For *in situ* annealing measurements shown in Figure 4, a 310 nm thick sample deposited at 325 K and 0.2 nm s^{-1} (shown in Figure 3A) was brought from room temperature to 335 K. For Figure 4, we took the starting time for the experiment as the time when the sample reached 335 K; the film was above T_g for no more than 10 seconds before this time. Images were collected at θ_{in} = 0.14° for 30 second exposures. Annealing times reported are the midpoint of each measurement. Several spots were used to avoid beam damage (SI text, Avoiding beam damage). After annealing, the sample was cooled to room temperature at ambient conditions and all five spots were re-measured to ensure consistency between spots. Smectic-like order integrations (Figure 4E) were performed as described above. Orientational order measurements (Figure 4F) were integrated with respect to azimuthal angle χ from q = 1.1 to 1.7 $Å^{-1}$.

Acknowledgements

This research was primarily supported by NSF through the University of Wisconsin Materials Research Science and Engineering Center (DMR-1720415). Use of the Stanford Synchrotron Radiation Lightsource, SLAC National Accelerator Laboratory, is supported by the U.S. Department of Energy, Office of Science, Office of Basic Energy Sciences under Contract No. DE-AC02-76SF00515. NEXAFS was undertaken on the Soft X-ray Spectroscopy beamline at the Australian Synchrotron, part of ANSTO. We thank Tim Dunn and Chris Tassone for assistance on Beamline 11-3.

References

1. Swallen SF, Kearns KL, Mapes MK, Kim YS, McMahon RJ, Ediger MD, Wu T, Yu L, Satija S (2007) Organic Glasses with Exceptional Thermodynamic and Kinetic Stability. *Science* 315(5810):353-356.
2. Tangpatjaroen C, Bagchi K, Martínez RA, Grierson D, Szlufarska I (2018) Mechanical Properties of Structure-Tunable, Vapor-Deposited TPD Glass. *J. Phys. Chem. C* 122(48):27775-27781.
3. Rodríguez-Tinoco C, Gonzalez-Silveira M, Ràfols-Ribé J, Lopeandía AF, Rodríguez-Viejo J (2015) Transformation kinetics of vapor-deposited thin film organic glasses: the role of stability and molecular packing anisotropy. *Phys. Chem. Chem. Phys.* 17(46):31195-31201.
4. Botto PA, Duckett RA, Ward IM (1987) The yield and thermoelastic properties of oriented poly(methyl methacrylate). *Polymer* 28(2):257-262.
5. Sun YH, Concustell A, Carpenter MA, Qiao JC, Rayment AW, Greer AL (2016) Flow-induced elastic anisotropy of metallic glasses. *Acta Mater.* 112:132-140.
6. Dalal SS, Walters DM, Lyubimov I, de Pablo JJ, Ediger MD (2015) Tunable molecular orientation and elevated thermal stability of vapor-deposited organic semiconductors. *Proc. Nat. Acad. Sci.* 112(14):4227-4232.
7. Yokoyama D (2011) Molecular orientation in small-molecule organic light-emitting diodes. *J. Mater. Chem.* 21:19187-19202.
8. Hellman F (1994) Surface-induced ordering: A model for vapor-deposition growth of amorphous materials. *Appl. Phys. Lett.* 64(15):1947-1949.
9. Ràfols-Ribé J, Will P-A, Hänisch C, Gonzalez-Silveira M, Lenk S, Rodríguez-Viejo J, Reineke S (2018) High-performance organic light-emitting diodes comprising ultrastable glass layers. *Sci. Adv.* 4(5).
10. Yasuda T, Fujita K, Tsutsui T, Geng Y, Culligan SW, Chen SH (2005) Carrier Transport Properties of Monodisperse Glassy-Nematic Oligofluorenes in Organic Field-Effect Transistors. *Chem. Mater.* 17(2):264-268.
11. Sirringhaus H, Wilson RJ, Friend RH, Inbasekaran M, Wu W, Woo EP, Grell M, Bradley DDC (2000) Mobility enhancement in conjugated polymer field-effect transistors through chain alignment in a liquid-crystalline phase. *Appl. Phys. Lett.* 77(3):406-408.
12. Menke SM, Holmes RJ (2015) Energy-Cascade Organic Photovoltaic Devices Incorporating a Host–Guest Architecture. *ACS Appl. Mater. Inter.* 7(4):2912-2918.
13. Gómez J, Jiang J, Gujral A, Huang C, Yu L, Ediger MD (2016) Vapor deposition of a smectic liquid crystal: highly anisotropic, homogeneous glasses with tunable molecular orientation. *Soft Matter* 12:2942-2947.
14. Yokoyama D, Sakaguchi A, Suzuki M, Adachi C (2009) Horizontal orientation of linear-shaped organic molecules having bulky substituents in neat and doped vacuum-deposited amorphous films. *Org. Electron.* 10(1):127-137.

15. Jiang J, Walters DM, Zhou D, Ediger MD (2016) Substrate temperature controls molecular orientation in two-component vapor-deposited glasses. *Soft Matter* 12:3265-3270.
16. Magliulo M, Mulla MY, Singh M, Macchia E, Tiwari A, Torsi L, Manoli K (2015) Printable and flexible electronics: from TFTs to bioelectronic devices. *J. Mater. Chem. C* 3(48):12347-12363.
17. Suga H, Seki S (1974) Thermodynamic investigation on glassy states of pure simple compounds. *J. Non-Cryst. Solids* 16(2):171-194.
18. Sorai M, Seki S (1971) Glassy Liquid Crystal of the Nematic Phase of N-(o-Hydroxy-p-methoxybenzylidene)-p-butylaniline. *Bull. Chem. Soc. Jpn.* 44(10):2887-2887.
19. Tsuji K, Sorai M, Seki S (1971) New Finding of Glassy Liquid Crystal – a Non-equilibrium State of Cholesteryl Hydrogen Phthalate. *Bull. Chem. Soc. Jpn.* 44(5):1452-1452.
20. Jerome B (1991) Surface effects and anchoring in liquid crystals. *Rep. Prog. Phys.* 54(3):391-451.
21. Gómez J, Gujral A, Huang C, Bishop C, Yu L, Ediger MD (2017) Nematic-like stable glasses without equilibrium liquid crystal phases. *J. Chem. Phys.* 146:054503.
22. Gujral A, Gómez J, Jiang J, Huang C, O'Hara KA, Toney MF, Chabinyc ML, Yu L, Ediger MD (2017) Highly Organized Smectic-like Packing in Vapor-Deposited Glasses of a Liquid Crystal. *Chem. Mater.* 29:849-858.
23. Gujral A, Gómez J, Ruan S, Toney MF, Bock H, Yu L, Ediger MD (2017) Vapor-Deposited Glasses with Long-Range Columnar Liquid Crystalline Order. *Chem. Mater.* 29(21):9110-9119.
24. Funahashi M, Hanna JI (2005) High Carrier Mobility up to 0.1 cm2 V–1 s–1 at Ambient Temperatures in Thiophene-Based Smectic Liquid Crystals. *Adv. Mater.* 17(5):594-598.
25. Eccher J, Zajaczkowski W, Faria GC, Bock H, von Seggern H, Pisula W, Bechtold IH (2015) Thermal Evaporation versus Spin-Coating: Electrical Performance in Columnar Liquid Crystal OLEDs. *ACS Appl. Mater. Inter.* 7:16374-16381.
26. Rivnay J, Mannsfeld SCB, Miller CE, Salleo A, Toney MF (2012) Quantitative Determination of Organic Semiconductor Microstructure from the Molecular to Device Scale. *Chem. Rev.* 112(10):5488-5519.
27. Gujral A, O'Hara KA, Toney MF, Chabinyc ML, Ediger MD (2015) Structural characterization of vapor-deposited glasses of an organic hole transport material with X-ray scattering. *Chem. Mater.* 27:3341-3348.
28. Benmore CJ, Mou Q, Benmore KJ, Robinson DS, Neuefeind J, Ilavsky J, Byrn SR, Yarger JL (2016) A SAXS-WAXS study of the endothermic transitions in amorphous or supercooled liquid itraconazole. *Thermochim. Acta* 644:1-5.
29. Teerakapibal R, Huang C, Gujral A, Ediger MD, Yu L (2018) Organic Glasses with Tunable Liquid-Crystalline Order. *Phys. Rev. Lett.* 120(5):055502.
30. Yu L (2016) Surface mobility of molecular glasses and its importance in physical stability. *Adv. Drug Deliv. Rev.* 100:3-9.
31. Bagchi K, Jackson NE, Gujral A, Huang C, Toney MF, Yu L, de Pablo JJ, Ediger MD (2019) Origin of Anisotropic Molecular Packing in Vapor-Deposited Alq3 Glasses. *J. Phys. Chem. Lett.* 10:164-170.

32. Liu T, Exarhos AL, Alguire EC, Gao F, Salami-Ranjbaran E, Cheng K, Jia T, Subotnik JE, Walsh PJ, Kikkawa JM, Fakhraai Z (2017) Birefringent Stable Glass with Predominantly Isotropic Molecular Orientation. *Phys. Rev. Lett.* 119:095502.
33. Stöhr J, Outka DA (1987) Determination of molecular orientations on surfaces from the angular dependence of near-edge x-ray-absorption fine-structure spectra. *Phys. Rev. B* 36(15):7891-7905.
34. Ehlert C, Holzweber M, Lippitz A, Unger WES, Saalfrank P (2016) A detailed assignment of NEXAFS resonances of imidazolium based ionic liquids. *Phys. Chem. Chem. Phys.* 18(12):8654-8661.
35. Hitchcock AP, Pocock M, Brion CE, Banna MS, Frost DC, McDowell CA, Wallbank B (1978) Inner shell excitation and ionization of the monohalobenzenes. *J. Electron Spectrosc.* 13(3):345-360.
36. Cooney RR, Urquhart SG (2004) Chemical Trends in the Near-Edge X-ray Absorption Fine Structure of Monosubstituted and Para-Bisubstituted Benzenes. *J. Phys. Chem. B* 108(47):18185-18191.
37. Urquhart SG, Ade H (2002) Trends in the Carbonyl Core (C 1S, O 1S) → π*C=O Transition in the Near-Edge X-ray Absorption Fine Structure Spectra of Organic Molecules. *J. Phys. Chem. B* 106(34):8531-8538.
38. Lyubimov I, Antony L, Walters DM, Rodney D, Ediger MD, de Pablo JJ (2015) Orientational anisotropy in simulated vapor-deposited molecular glasses. *J. Chem. Phys.* 143:094502.
39. Walters DM, Antony L, de Pablo JJ, Ediger MD (2017) Influence of Molecular Shape on the Thermal Stability and Molecular Orientation of Vapor-Deposited Organic Semiconductors. *J. Phys. Chem. Lett.* 8(14):3380-3386.
40. Pershan PS, Braslau A, Weiss AH, Als-Nielsen J (1987) Smectic layering at the free surface of liquid crystals in the nematic phase: X-ray reflectivity. *Phys. Rev. A* 35(11):4800-4813.
41. Zola RS, Bisoyi HK, Wang H, Urbas AM, Bunning TJ, Li Q (2019) Dynamic Control of Light Direction Enabled by Stimuli-Responsive Liquid Crystal Gratings. *Adv. Mater.* 31(7):1806172.
42. Kearns KL, Swallen SF, Ediger MD, Wu T, Sun Y, Yu L (2008) Hiking down the Energy Landscape: Progress Toward the Kauzmann Temperature via Vapor Deposition. *J. Phys. Chem. B* 112(16):4934-4942.
43. Kearns KL, Krzyskowski P, Devereaux Z (2017) Using deposition rate to increase the thermal and kinetic stability of vapor-deposited hole transport layer glasses via a simple sublimation apparatus. *J. Chem. Phys.* 146(20):203328.
44. Adrjanowicz K, Kaminski K, Wlodarczyk P, Grzybowska K, Tarnacka M, Zakowiecki D, Garbacz G, Paluch M, Jurga S (2013) Molecular dynamics of the supercooled pharmaceutical agent posaconazole studied via differential scanning calorimetry and dielectric and mechanical spectroscopies. *Mol. Pharm.* 10:3934-3945.
45. Leadbetter AJ, Norris EK (1979) Distribution functions in three liquid crystals from X-ray diffraction measurements. *Mol. Phys.* 38(3):669-686.
46. Regan MJ, Kawamoto EH, Lee S, Pershan PS, Maskil N, Deutsch M, Magnussen OM, Ocko BM, Berman LE (1995) Surface Layering in Liquid Gallium: An X-Ray Reflectivity Study. *Phys. Rev. Lett.* 75(13):2498-2501.

47. Youn Y, Yoo D, Song H, Kang Y, Kim KY, Jeon SH, Cho Y, Chae K, Han S (2018) All-atom simulation of molecular orientation in vapor-deposited organic light-emitting diodes. *J. Mater. Chem. C* 6(5):1015-1022.
48. Chen Z, Sepúlveda A, Ediger MD, Richert R (2013) Dynamics of glass-forming liquids. XVI. Observation of ultrastable glass transformation via dielectric spectroscopy. *J. Chem. Phys.* 138(12):12A519.
49. Moore AR, Huang G, Wolf S, Walsh PJ, Fakhraai Z, Riggleman RA (2019) Effects of microstructure formation on the stability of vapor-deposited glasses. *Proc. Nat. Acad. Sci.* 116(13):5937.
50. Sadati M, Ramezani-Dakhel H, Bu W, Sevgen E, Liang Z, Erol C, Rahimi M, Taheri Qazvini N, Lin B, Abbott NL, Schlossman ML, de Pablo JJ (2017) Molecular Structure of Canonical Liquid Crystal Interfaces. *J. Am. Chem. Soc.* 139:3841-3850.
51. Philp Chen H-M, Ou JJ, Chen SH (2014) Glassy Liquid Crystals as Self-Organized Films for Robust Optoelectronic Devices. *Nanoscience with Liquid Crystals*, ed Li Q (Springer, New York), pp 179-208.
52. Eccher J, Faria GC, Bock H, Von Seggern H, Bechtold IH (2013) Order Induced Charge Carrier Mobility Enhancement in Columnar Liquid Crystal Diodes. *ACS Appl. Mater. Inter.* 5:11935-11943.
53. Zimmermann U, Schnitzler G, Wüstenhagen V, Karl N, Dudde R, Koch EE, Umbach E (2000) NEXAFS and ARUP Spectroscopy of an Organic Single Crystal: α-Perylene. *Mol. Cryst. Liq. Crys. A* 339(1):231-259.
54. Oosterhout SD, Savikhin V, Zhang J, Zhang Y, Burgers MA, Marder SR, Bazan GC, Toney MF (2017) Mixing Behavior in Small Molecule:Fullerene Organic Photovoltaics. *Chem. Mater.* 29(7):3062-3069.
55. Ilavsky J (2012) Nika: software for two-dimensional data reduction. *J. Appl. Crystallogr.* 45(2):324-328.
56. Zhang F, Ilavsky J, Long GG, Quintana JPG, Allen AJ, Jemian PR (2010) Glassy Carbon as an Absolute Intensity Calibration Standard for Small-Angle Scattering. *Metall. Mater. Trans. A* 41(5):1151-1158.
57. Mannsfeld SCB, Virkar A, Reese C, Toney MF, Bao Z (2009) Precise Structure of Pentacene Monolayers on Amorphous Silicon Oxide and Relation to Charge Transport. *Adv. Mater.* 21(22):2294-2298.
58. Gann E, McNeill CR, Tadich A, Cowie BCC, Thomsen L (2016) Quick AS NEXAFS Tool (QANT): a program for NEXAFS loading and analysis developed at the Australian Synchrotron. *Journal of Synchrotron Radiation* 23(1):374-380.

Supporting information for "Vapor deposition of a nonmesogen prepares highly structured organic glasses" by Camille Bishop, Jacob Thelen, Eliot Gann, Michael F. Toney, Lian Yu, Dean M. DeLongchamp, M. D. Ediger.

SI Section 1. NEXAFS orientation and peak analysis.

The normalized NEXAFS data for posaconazole can be described by nine Gaussian peaks and a step-edge, as shown in Figure S1.

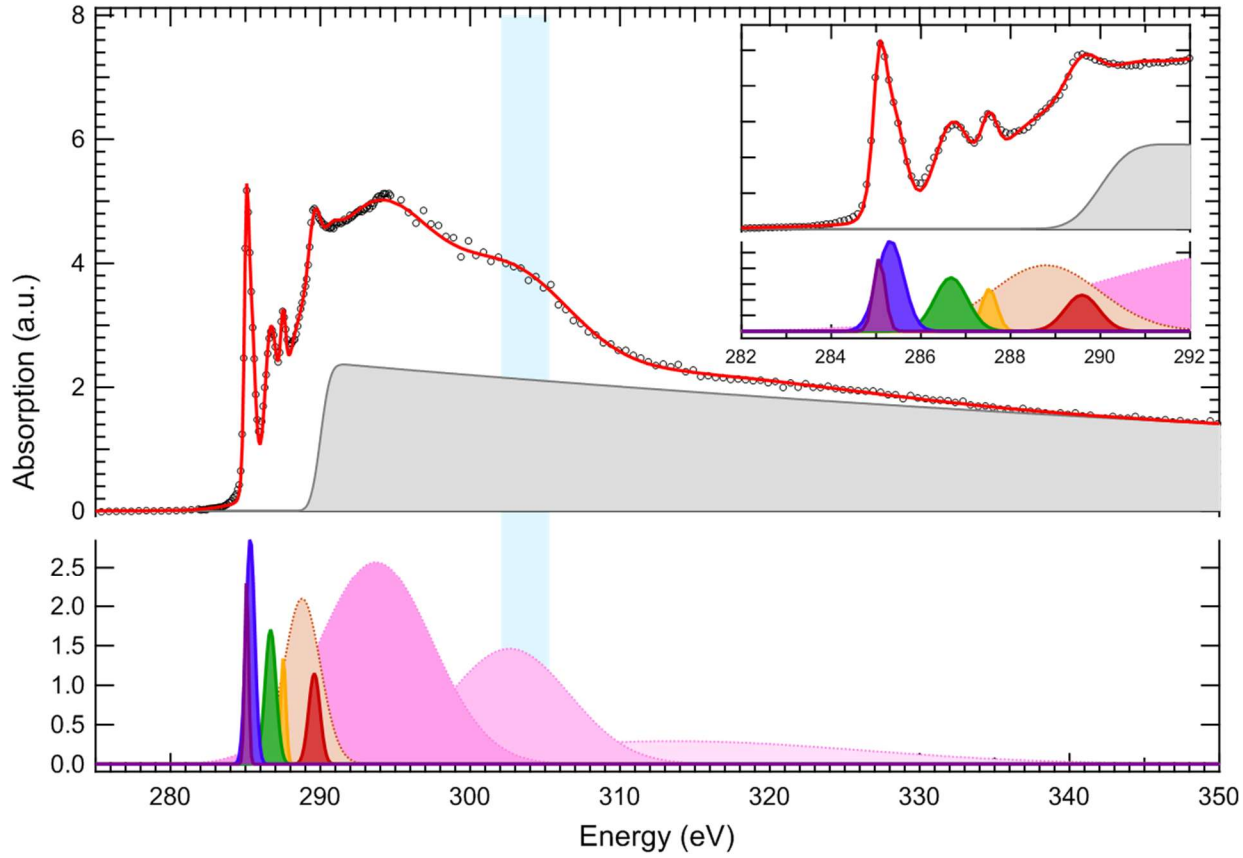

Figure S1. Magic-angle (θ_{in} = 55°) NEXAFS data (black circles) and fit (red curve) for posaconazole. The nine Gaussian contributions to the fit, as well as the step-edge contribution are also plotted as shaded regions for reference.

The incident-angle-dependent NEXAFS data for the liquid-cooled glass of posaconazole (deposited at 334K) were fit by adjusting only the peak heights for the Gaussian peaks shown in Figure S1. The fits were performed using the multipeak analysis in QANT (1) and are shown in Figure S2.

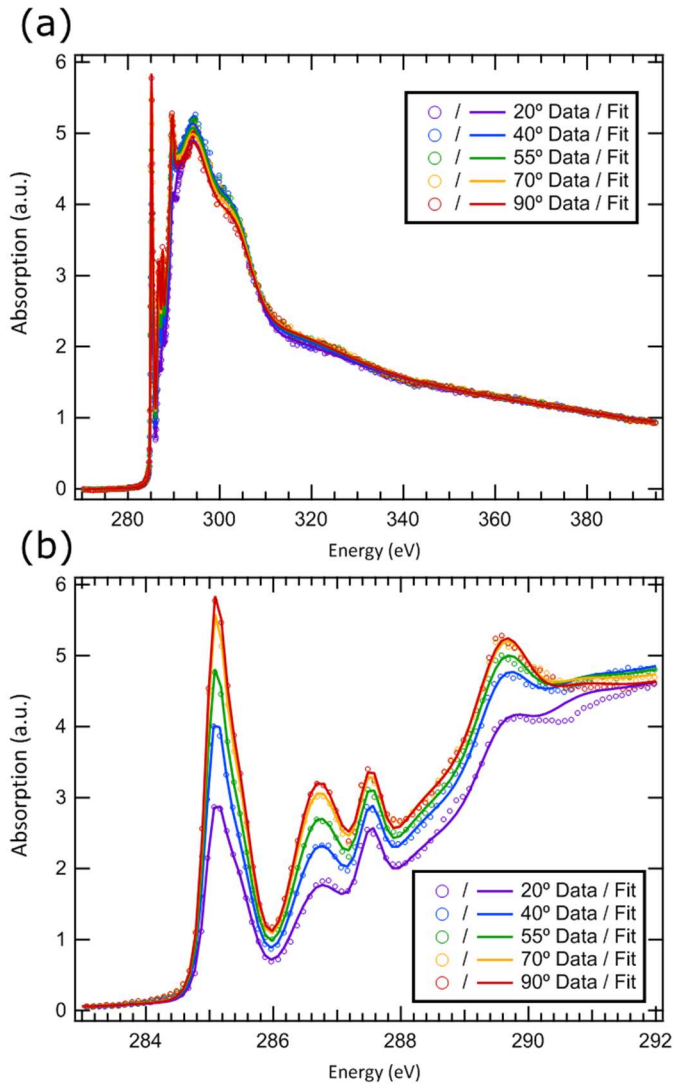

Figure S2. Incident-angle-dependent NEXAFS data (circles) and fits (curves) for posaconazole deposited at 334K. (a) Full range of data fitted by the Gaussian and step-edge functions shown in Figure S1, and (b) highlight of the 1s →π* resonance region.

We focus on the 5 sharpest, lowest-energy 1s→π* resonances. The integrated peak intensity as a function of incidence angle was fit to Equation S1:

$$I(\gamma,\theta) = A * \left\{\frac{2}{3}\left[1 - \frac{1}{4}(3cos^2\theta - 1)(3cos^2\gamma - 1)\right]\right\} \text{ (Equation S1)}$$

where θ is the incidence angle of the radiation, γ is the angle between the molecular long-axis and the substrate normal, and A is a normalization factor. Equation S1 is equivalent to Stöhr's

plane symmetry formula 9.17a (2). The plane symmetry formula provides the correct molecular long-axis orientation because each of the 1s→π* resonances, which have vector symmetry normal to the plane of the conjugated rings (equally adopt all orientations orthogonal to the molecular long axis), effectively traces out a plane with the molecular long axis as its surface normal. Thus, the orientation of the effective plane determined by Equation S1 provides the orientation of the long axis of the molecule. A representative fit to Equation S1 from the peak centered at 286.7 eV is shown in Figure S3. The fit result indicates that on average, the long-axis is tilted ~33° from the surface normal. Each of the 1s→π* resonance peaks were fitted as shown in Figure S3 using the QANT macro (1), and the resulting long-axis orientation results are shown in Table S1.

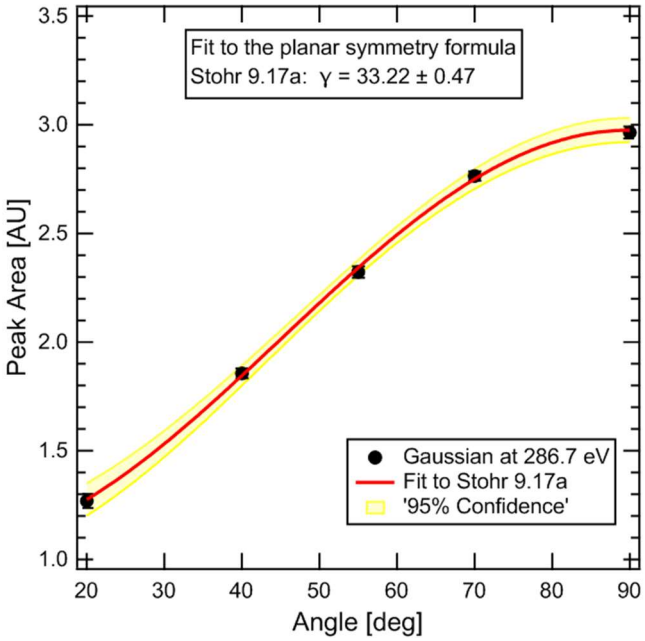

Figure S3. Integrated peak intensities of 1s→π* transitions centered at 286.7 eV (black circles), with fit to Equation S1 (red curve). The gold shaded band indicates the 95% confidence interval for the fit.

Peak Position (eV)	γ - Stohr 9.17a (degrees)
285.1	35.4 +/- 0.6
285.3	37.8 +/- 0.4
286.7	33.2 +/- 0.5
287.5	46 +/- 1
289.6	43.1 +/- 0.7

Table S1. Long-axis orientation results from fitting the angle-dependent peak areas to Equation S1.

In order to assign the 1s→π* resonances at 286.7 eV and 287.5 eV in the NEXAFS spectra, in Figure S4 we provide the magic-angle (θ_{in} = 55°) NEXAFS data for posaconazole and the related molecule, itraconazole. These data were collected using the NEXAFS endstation at the SST-1 beamline at NSLS-II. The data were collected in partial electron yield mode (PEY) using a channeltron detector with a -50V grid bias. The data were processed in QANT (1): the channeltron values were corrected for the incident flux using the gold mesh channel, and then the spectra were normalized to 0 prior to resonant absorption and 1 at energies well above the absorption edge. The major chemical difference between the two molecules is that itraconazole has a dichlorinated phenyl ring, while posaconazole has a difluorinated phenyl ring. The 1s →π* transition resonances for C=CCl and C=CF bonds on substituted benzene rings are expected to occur at 286.3 eV and 287.5 eV, respectively (3). The absence of a peak at 287.5 eV in the itraconazole data allows us to assign the 287.5 eV peak present in the posaconazole spectra to the fluorine-substituted carbons. This assignment is further supported by the increase in peak intensity near 286.3 eV in the itraconazole spectra, which we attribute to the 1s →π* resonance for the chlorine-substituted carbons. Thus the 286.7 eV peak in the posaconazole spectra likely contains contributions from the triazole and triazolone C=N 1s →π* resonances, as well as the C=CN and possibly C=CO 1s →π* resonances from the substituted aromatic rings in the core of the molecule.

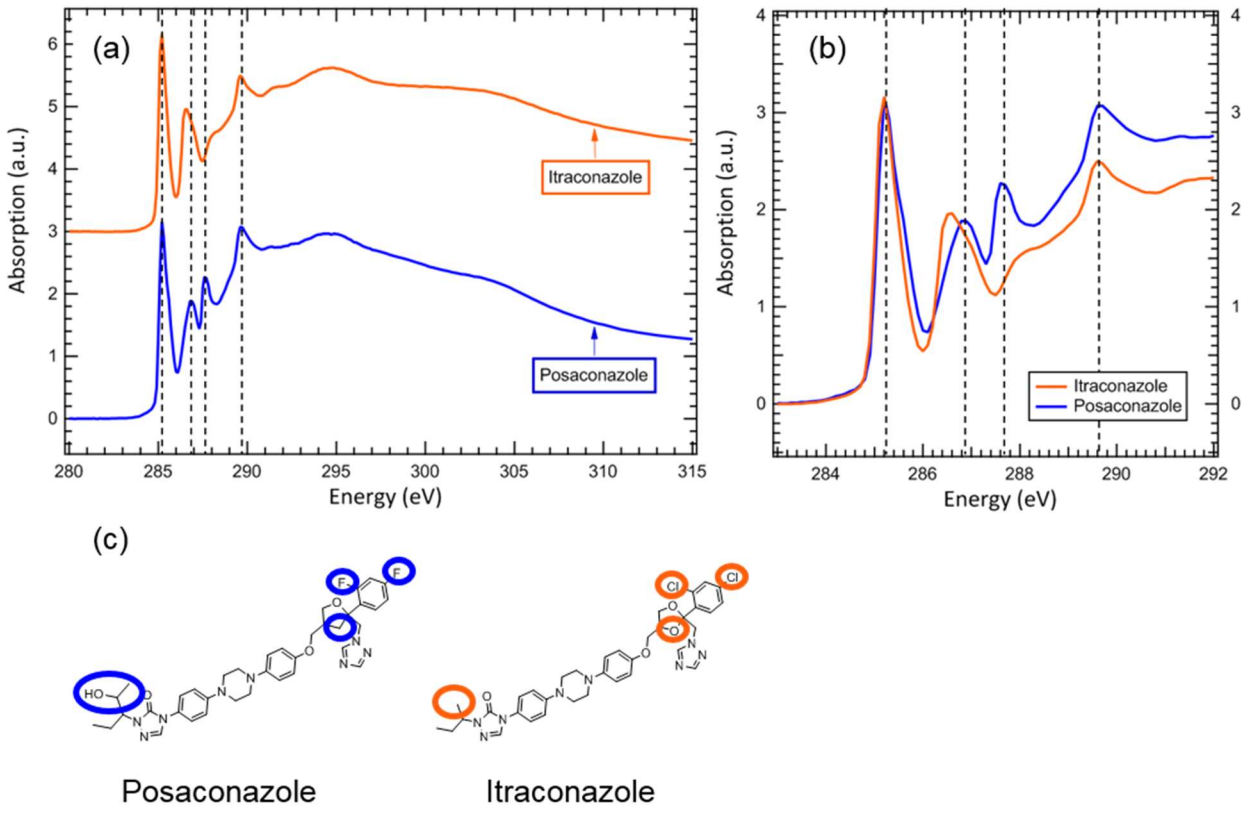

Figure S4. NEXAFS spectra for itraconazole and posaconazole. In (a), the spectra are offset for clarity, and in (b) the spectra are overlaid in the 1s →π* region for comparison. (c) shows the molecular structures of posaconazole and itraconazole, with differences circled.

SI Section 2. Bulk orientation of liquid-cooled glass.

Ellipsometry was performed on the sample used for NEXAFS at 9 points using 7 incident angles. Data between 500 and 1000 nm were fit to an anisotropic Cauchy model, in which the ordinary and extraordinary refractive indices are given, respectively, by

$$n_o = A_o + \frac{B}{\lambda^2} \text{ and } n_e = A_e + \frac{B}{\lambda^2} \quad \text{(Equation S2)}$$

Birefringence is equal to $n_e - n_o$. Over nine points, the average birefringence was 0.0006 ± 0.0008, with a minimum value of -0.0008 and a maximum value of 0.0015. These values are consistent with an isotropic film.

SI Section 3. Bulk orientational order of vapor-deposited glass.

We quantify the bulk orientational order to compare to the NEXAFS. We stress that the NEXAFS data may not be an exact measure of orientation at only the surface monolayer, since the probe depth of 6 nm is equal to approximately two molecular lengths. We also note that the GIWAXS order parameter does not report the molecular orientation, but rather the orientational order of anisotropic molecular packing. Therefore, the two measures of order can be compared only qualitatively.

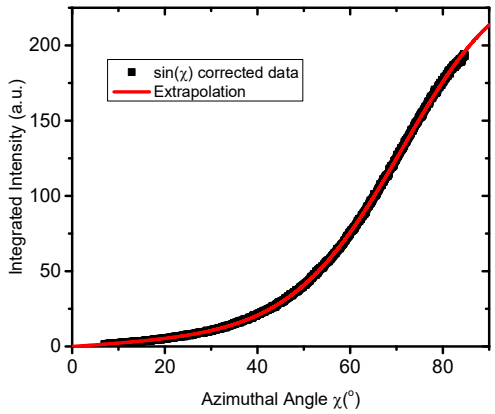

Figure S5. Radial integration of GIWAXS from q = 1.1 to 1.7 Å^{-1} of an extremely ordered glass of posaconazole deposited at 325 K and 0.02 nm s^{-1}.

A GIWAXS order-parameter for the scattering feature at $q \approx 1.3$ Å^{-1} was calculated according to Gujral et. al. (4), with a result of -0.28. S_{GIWAXS} quantifies the distribution of scattering intensity at an azimuthal angle χ (defined as 0° along q_z) by

$$S_{GIWAXS} = \frac{1}{2}(3\langle cos^2\chi\rangle - 1) \qquad \text{(Equation S3).}$$

S_{GIWAXS} can vary between the limits of +1 and -0.5. The order parameter of -0.28 indicates a concentration of intensity from scattering of the $q \approx 1.3$ Å^{-1} feature near the q_{xy} direction. This concentration of scattering nearly in-plane is consistent with a picture in which mostly vertically oriented posaconazole molecules pack laterally in-plane with a nearest-neighbor distance of ~ 0.48 nm. The large width of the peak, with a coherence length of 2.9 nm as stated in the main text, is consistent with an amorphous or liquid-like packing.

SI Section 4. Avoiding beam damage.

To minimize beam damage, measurements were made at four different spots during annealing. Exposures lasted 30 seconds to minimize beam damage while optimizing signal-to-noise and time resolution. Before annealing, five spots were measured and found to be structurally equivalent, with 2D patterns shown in Figure S6. To quantify the orientational order, we calculate the GIWAXS order parameter (27) for each spot before and after annealing, shown in table S2. The order parameters before and after all match within error, so we combine data from different spots into one *in situ* measurement. One spot was not measured at all during annealing; after the sample was cooled, the spot's structure was isotropic. The evolution of molecular packing observed is therefore a result of the thermal treatment, and not any X-ray damage.

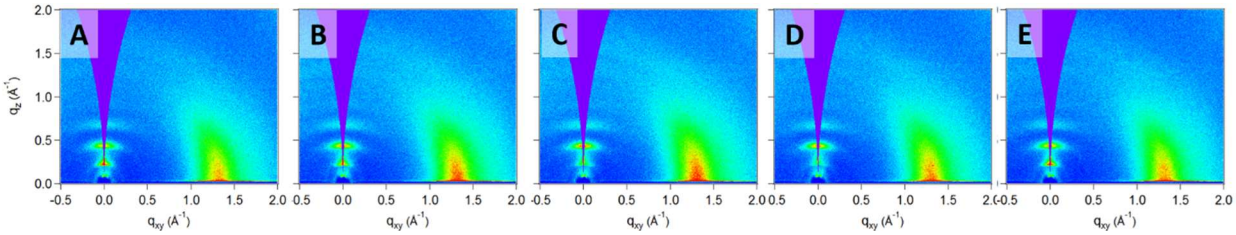

Figure S6. GIWAXS before annealing of five distinct spots.

Spot	S_{GIWAXS} before	S_{GIWAXS} after
A	-0.283	0.006
B	-0.268	0.007
C	-0.264	0.004
D	-0.272	0.004
E	-0.279	0.005

Table S2. GIWAXS order parameter before and after annealing for all five spots.

As-deposited glasses shown in Figures 1 and 3 are not damaged by the beam, as illustrated by the following test. For a sample prepared at the same conditions as the one shown in Figure S6C, one 45-second exposure at $\theta_{in} = 0.14°$ was taken before other measurements. It then received 600 s of X-ray exposure, after which a final 45-second exposure at $\theta_{in} = 0.14°$ was taken. Within measurement error, the two 45-second exposures had identical amounts of orientational and translational order.

References

1. Gann E, McNeill CR, Tadich A, Cowie BCC, Thomsen L (2016) Quick AS NEXAFS Tool (QANT): a program for NEXAFS loading and analysis developed at the Australian Synchrotron. *J. Synchrotron Radiat.* 23(1):374-380.
2. Stöhr J (1992) NEXAFS Spectroscopy (Springer-Verlag, Berlin) 2nd Ed.
3. Cooney RR, Urquhart SG (2004) Chemical Trends in the Near-Edge X-ray Absorption Fine Structure of Monosubstituted and Para-Bisubstituted Benzenes. *J. Phys. Chem. B* 108(47):18185-18191.
4. Gujral A, O'Hara KA, Toney MF, Chabinyc ML, Ediger MD (2015) Structural characterization of vapor-deposited glasses of an organic hole transport material with X-ray scattering. *Chem. Mater.* 27:3341-3348.